



Article

# Calcination Method Synthesis of SnO<sub>2</sub>/g-C<sub>3</sub>N<sub>4</sub> Composites for a High-Performance Ethanol Gas Sensing Application

Jianliang Cao <sup>1</sup>, Cong Qin <sup>1</sup>, Yan Wang <sup>2,\*</sup>, Bo Zhang <sup>1</sup>, Yuxiao Gong <sup>1</sup>, Huoli Zhang <sup>1</sup>, Guang Sun <sup>1</sup>, Hari Bala <sup>1</sup> and Zhanying Zhang <sup>1,\*</sup>

<sup>1</sup> School of Chemistry and Chemical Engineering, Henan Polytechnic University, Jiaozuo 454000, China; caojianliang@hpu.edu.cn (J.C.); qincongxy@163.com (C.Q.); zhb@hpu.edu.cn (B.Z.); gyx201311@163.com (Y.G.); zhanghuoli@hpu.edu.cn (H.Z.); mcsunguang@hpu.edu.cn (G.S.); hari@hpu.edu.cn (H.B.)

<sup>2</sup> School of Safety Science and Engineering, State Key Laboratory Cultivation Base for Gas Geology and Gas Control, Henan Polytechnic University, Jiaozuo 454000, China

\* Correspondence: yanwang@hpu.edu.cn (Y.W.); zhangzy@hpu.edu.cn (Z.Z.); Tel.: +86-391-398-7440 (Y.W. & Z.Z.)

Academic Editor: Guozhen Liu

Received: 7 February 2017; Accepted: 12 April 2017; Published: 29 April 2017

**Abstract:** The SnO<sub>2</sub>/g-C<sub>3</sub>N<sub>4</sub> composites were synthesized via a facile calcination method by using SnCl<sub>4</sub>·5H<sub>2</sub>O and urea as the precursor. The structure and morphology of the as-synthesized composites were characterized by the techniques of X-ray diffraction (XRD), the field-emission scanning electron microscopy and transmission electron microscopy (SEM and TEM), energy dispersive spectrometry (EDS), thermal gravity and differential thermal analysis (TG-DTA), and N<sub>2</sub>-sorption. The analysis results indicated that the as-synthesized samples possess the two dimensional structure. Additionally, the SnO<sub>2</sub> nanoparticles were highly dispersed on the surface of the g-C<sub>3</sub>N<sub>4</sub> nanosheets. The gas-sensing performance of the as-synthesized composites for different gases was tested. Moreover, the composite with 7 wt % g-C<sub>3</sub>N<sub>4</sub> content (SnO<sub>2</sub>/g-C<sub>3</sub>N<sub>4</sub>-7) SnO<sub>2</sub>/g-C<sub>3</sub>N<sub>4</sub>-7 exhibits an admirable gas-sensing property to ethanol, which possesses a higher response and better selectivity than that of the pure SnO<sub>2</sub>-based sensor. The high surface area of the SnO<sub>2</sub>/g-C<sub>3</sub>N<sub>4</sub> composite and the good electronic characteristics of the two dimensional graphitic carbon nitride are in favor of the elevated gas-sensing property.

**Keywords:** graphitic carbon nitride; SnO<sub>2</sub>; calcination method; SnO<sub>2</sub>/g-C<sub>3</sub>N<sub>4</sub> composite; ethanol gas sensing

## 1. Introduction

In recent years, poisonous and harmful gases of industrial production have frequently leaked. Meanwhile, organic poisonous gases, such as methylbenzene and formaldehyde, volatilize from furniture and newly-decorated houses. As a result, it severely threatens the health of mankind [1–4]. Therefore, there is the need for an effective and necessary method for detecting the vaporable substances. In the past several years, considerable attentions have been dedicated to metal-oxide semiconductor (MOS) material-based gas sensors. Various metal-oxide semiconductors (MOS), such as SnO<sub>2</sub> [5], ZnO [6], CuO [7], α-Fe<sub>2</sub>O<sub>3</sub> [8], Co<sub>3</sub>O<sub>4</sub> [9], MnO<sub>2</sub> [10], WO<sub>3</sub> [11], In<sub>2</sub>O<sub>3</sub> [12], and NiO [13], are widely used as gas sensors. These gas sensors exhibited unique performances, including a low-cost, small size, and fast response and recovery time. SnO<sub>2</sub>, a typical n-type metal-oxide semiconductor with a rutile crystalline structure, is widely used to detect different kinds of gases such as ethanol [14], formaldehyde [15], acetone [16], nitrogen dioxide [17], etc. These are all due to their remarkable characteristics such as

their good chemical and physical stability, non-pollution property, low-energy feature, use of simple preparation, and so on.

The most remarkable characteristic of SnO<sub>2</sub> is that the resistance varies when it is exposed to different types of target gases. As a rule, the resistance value of SnO<sub>2</sub> decreases when it is exposed in reducing gases, and conversely, it increases under the oxidizing gases. As we all know, there are many oxygen vacancies of SnO<sub>2</sub> which are in favor of the process of gas adsorption. In general, it has a better gas-sensing performance with a higher concentration of oxygen vacancies. Nonetheless, there are some significant defects which restricts its application in gas sensors. For instance, a high working temperature, long response and recovery time, high resistance, and easy agglomeration draw the attention of researchers. In order to overcome these shortcomings, it is necessary to explore an electroconductive intermediate to support SnO<sub>2</sub> nanoparticles, in order to improve the electrical conductivity and dispersity. Therefore, many two-dimensional (2D) carbon materials are widely used as intermediates [18–20]. Graphene, a unilaminar sp<sup>2</sup>-hybridized carbon atoms configuration, exhibits an excellent performance, including a large specific surface area, better electronic conductivity, and superior stability. On account of these advantages, graphene and reduced graphene oxide are widely used as gas-sensing materials to detect different kinds of gases. Different metal-oxide decorated graphene nanocomposite gas sensors were reported and exhibited outstanding gas-sensing performances [21–24]. However, the process of preparing GO and r-GO is complicated and high-cost. Hence, it is necessary to explore a novel 2D structure material with graphene.

Recently, graphitic carbon nitride (g-C<sub>3</sub>N<sub>4</sub>) has attracted increasing attention due to its high photology and chemical stability, facile preparation, high specific surface area, and nontoxicity [25–28]. In general, g-C<sub>3</sub>N<sub>4</sub> is readily synthesized by calcining abundant nitrogen-rich precursors such as melamine, dicyandiamide, and urea. It has been widely used in fields such as photocatalysis, degradation, and energy storage materials [29–31]. Until now, there are few reports on the application of g-C<sub>3</sub>N<sub>4</sub> in the field of sensors. Zeng et al. have successfully prepared the α-Fe<sub>2</sub>O<sub>3</sub>/g-C<sub>3</sub>N<sub>4</sub> nanocomposite through a facile refluxing method for the cataluminescence sensing of H<sub>2</sub>S [32]. Zhang et al. have developed a novel fluorescence sensor based on a g-C<sub>3</sub>N<sub>4</sub>/MnO<sub>2</sub> sandwich nanocomposite for the rapid and selective sensing of glutathione [33]. Moreover, CeO<sub>2</sub>/g-C<sub>3</sub>N<sub>4</sub> composites with high photocatalytic activity have been synthesized successfully [34]. To the best of the authors' knowledge, SnO<sub>2</sub>/g-C<sub>3</sub>N<sub>4</sub> based sensors have yet not been reported in the literature.

In this work, we report a facile calcination approach to synthesize different mass ratios of SnO<sub>2</sub>/g-C<sub>3</sub>N<sub>4</sub> composites for ethanol sensing. The gas-sensing properties, including the selectivity, stability, and sensitivity, of SnO<sub>2</sub>/g-C<sub>3</sub>N<sub>4</sub> to ethanol, were investigated. As a result, the SnO<sub>2</sub>/g-C<sub>3</sub>N<sub>4</sub> composite-based sensor exhibited a higher response value and better selectivity to ethanol than that of the pure SnO<sub>2</sub> nanoparticle-based sensor. The mechanism of the as-prepared sample gas-sensing to ethanol was discussed, in detail.

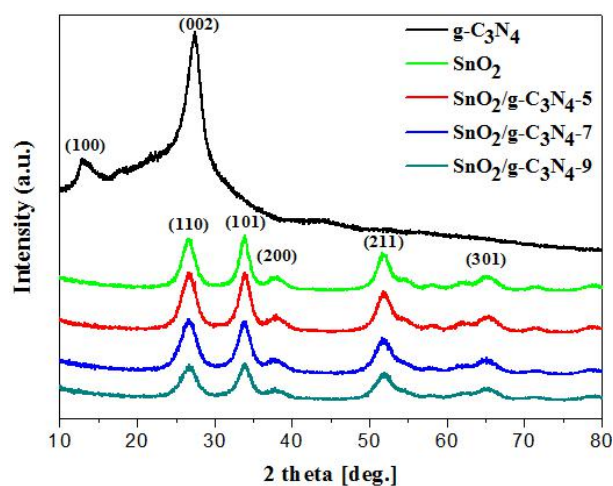
## 2. Results and Discussion

### 2.1. Sample Characterization

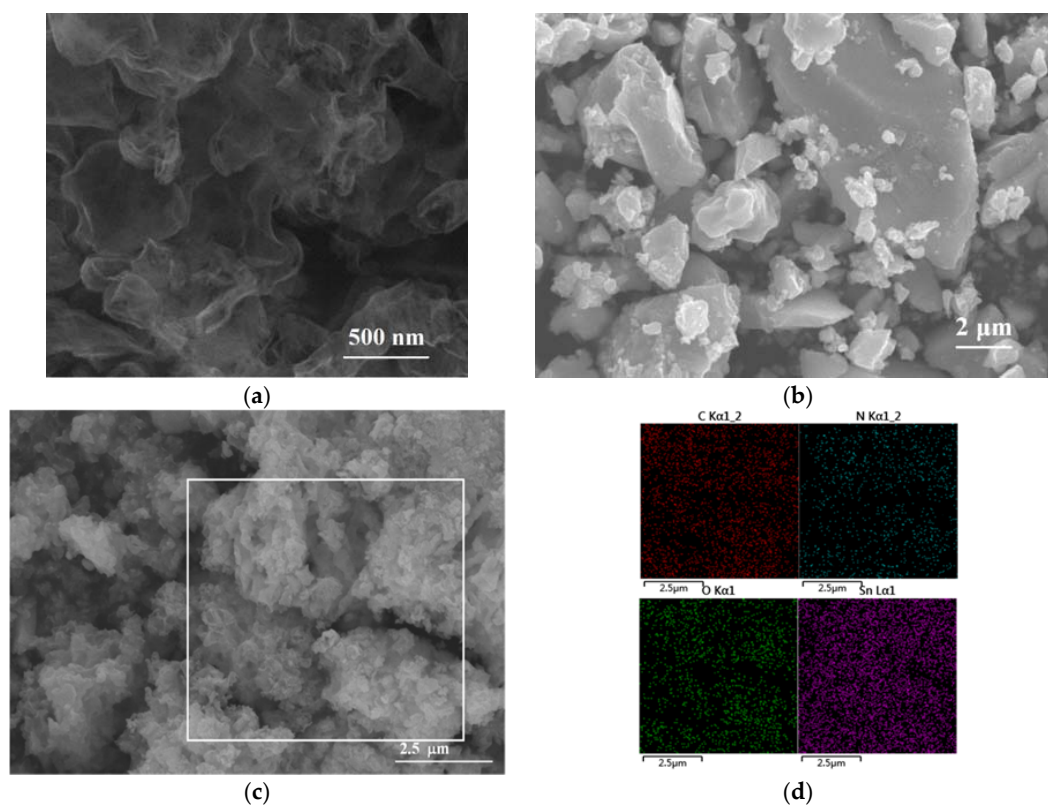
Figure 1 shows the XRD patterns of the as-prepared pure SnO<sub>2</sub> particles and SnO<sub>2</sub>/g-C<sub>3</sub>N<sub>4</sub> composites. As demonstrated by the curves, five distinct diffraction peaks around 26.6°, 33.8°, 37.9°, 51.7°, and 65.9° can be seen, which correspond to (110), (101), (200), (211), and (301) planes of the tetragonal rutile structure SnO<sub>2</sub> (JCPDS Card No. 41-1445), respectively. However, the diffraction peaks of g-C<sub>3</sub>N<sub>4</sub> in the SnO<sub>2</sub>/g-C<sub>3</sub>N<sub>4</sub> composites are not observed in the curves. This may be due to the relatively small content of g-C<sub>3</sub>N<sub>4</sub> in the composites. Another reason is that the peak around 27.5° of g-C<sub>3</sub>N<sub>4</sub> is overlapped by the peak around 26.6° of SnO<sub>2</sub>.

The SEM images of the g-C<sub>3</sub>N<sub>4</sub>, SnO<sub>2</sub>, and SnO<sub>2</sub>/g-C<sub>3</sub>N<sub>4</sub>-7 composites are displayed in Figure 2. Figure 2a displays the SEM image of the g-C<sub>3</sub>N<sub>4</sub> sample. We can see many wrinkles on the edge of the thin layers, which represents the nanosheet structure. Figure 2b shows many SnO<sub>2</sub> particles

agglomerated together with different sizes. This phenomenon indicates that pure SnO<sub>2</sub> particles are easy to agglomerate, which is harmful to the process of gas adsorption. As shown in Figure 2c, many nanoparticles are attached to the g-C<sub>3</sub>N<sub>4</sub> nanosheet. This could be beneficial to improving the gas-sensing properties. Figure 2d illustrates the typical EDS mappings of the SnO<sub>2</sub>/g-C<sub>3</sub>N<sub>4</sub>-7 composite recorded from the surface area that is observed in Figure 2c, in which four elements of C, N, Sn, and O are concurrently existent. It can be concluded that SnO<sub>2</sub> and g-C<sub>3</sub>N<sub>4</sub> are coexistent in the composite.

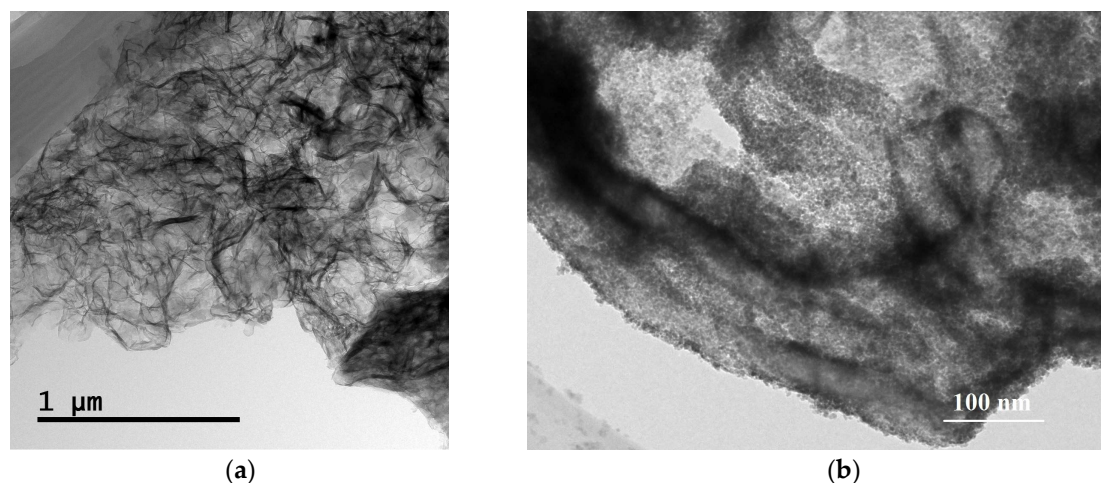


**Figure 1.** XRD patterns of the g-C<sub>3</sub>N<sub>4</sub>, SnO<sub>2</sub>, SnO<sub>2</sub>/g-C<sub>3</sub>N<sub>4</sub>-5, SnO<sub>2</sub>/g-C<sub>3</sub>N<sub>4</sub>-7, and SnO<sub>2</sub>/g-C<sub>3</sub>N<sub>4</sub>-9 composites.



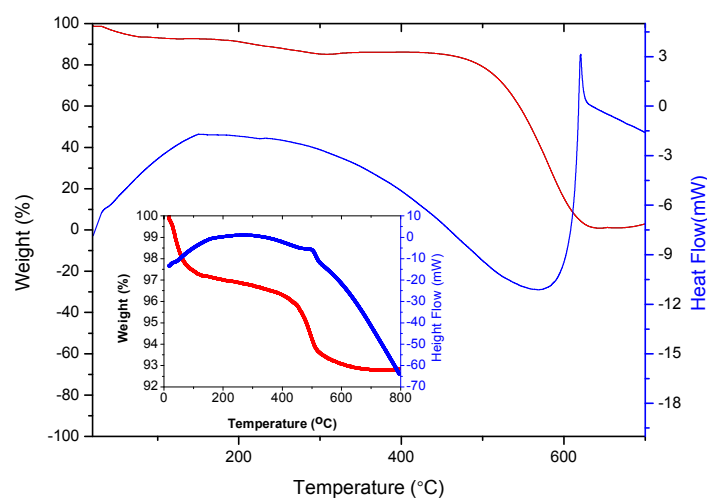
**Figure 2.** SEM images of (a) g-C<sub>3</sub>N<sub>4</sub>, (b) SnO<sub>2</sub> and (c) SnO<sub>2</sub>/g-C<sub>3</sub>N<sub>4</sub>-7 composite, (d) the EDS mappings of C, N, O, and Sn elements related to the selected area in (c).

Figure 3 shows the TEM images of  $g\text{-C}_3\text{N}_4$  and the  $\text{SnO}_2/g\text{-C}_3\text{N}_4\text{-7}$  composite. We can clearly see from Figure 3a that there are a lot of folds which seem like floccules, clearly demonstrating the existence of the  $g\text{-C}_3\text{N}_4$  nanosheet. The lines represent the stacked rolled edges of the nanosheet structure. As seen from Figure 3b, the  $\text{SnO}_2$  particles are highly dispersed on the surface of the  $g\text{-C}_3\text{N}_4$  nanosheet. This overcame the disadvantage of an easy agglomeration of  $\text{SnO}_2$  particles and further enhanced the specific surface area. Therefore, this test identifies it as an excellent candidate for gas-sensing materials.



**Figure 3.** TEM images of (a)  $g\text{-C}_3\text{N}_4$  and (b)  $\text{SnO}_2/g\text{-C}_3\text{N}_4\text{-7}$  composite.

TG-DTA was carried out to reveal the weight change situation of  $g\text{-C}_3\text{N}_4$  and  $\text{SnO}_2/g\text{-C}_3\text{N}_4\text{-7}$ . The temperature range is from room temperature to  $700\text{ }^\circ\text{C}$ , and the heating rate is  $10\text{ }^\circ\text{C}\cdot\text{min}^{-1}$ . As is shown in Figure 4, the red and blue lines correspond to weight and heat flow curves, respectively. The first agravity peak is between  $100\text{ }^\circ\text{C}$  and  $300\text{ }^\circ\text{C}$ , which is due to the desorption of moisture and the solvent. The second agravity peak is between  $400\text{ }^\circ\text{C}$  and  $600\text{ }^\circ\text{C}$ , which is due to the combustion of  $g\text{-C}_3\text{N}_4$  in air. The inset in Figure 4 is the TG-DTA profiles of  $\text{SnO}_2/g\text{-C}_3\text{N}_4\text{-7}$ . The agravic peak below  $400\text{ }^\circ\text{C}$  is due to the desorption of solvent, and the remanent content of the composite is 92% after the combustion of  $g\text{-C}_3\text{N}_4$ . This result demonstrated that  $g\text{-C}_3\text{N}_4$  was not decomposed at the optimum temperature of  $300\text{ }^\circ\text{C}$  in the process of testing the gas-sensing properties.



**Figure 4.** TG-DTA profiles of the  $g\text{-C}_3\text{N}_4$  and  $\text{SnO}_2/g\text{-C}_3\text{N}_4\text{-7}$  composite.

Figure 5 depicts the  $N_2$  adsorption-desorption isotherms and the corresponding pore size distribution of the as-prepared  $SnO_2$  and  $SnO_2/g-C_3N_4$ -7 samples. It can be seen from Figure 5a that the isotherms of the two samples show type IV, which are the typical characteristics of mesoporous materials according to the IUPAC. The well-defined hysteresis loop belonging to the  $H_3$ -type clearly indicates the existence of an aggregation of the laminated structure with a narrow slit formed by the  $g-C_3N_4$  and  $SnO_2$  nanoparticles. Figure 5b displays the corresponding pore size distribution of the two samples. It can be clearly seen that the pore diameter of  $SnO_2$  and  $SnO_2/g-C_3N_4$  are relatively small and that the majority concentrate upon 4.54 nm and 3.79 nm, respectively, according to the DFT method. The BET calculated results show that the specific surface area of the  $SnO_2$  and  $SnO_2/g-C_3N_4$ -7 samples are  $94.3 \text{ m}^2 \cdot \text{g}^{-1}$  and  $132.5 \text{ m}^2 \cdot \text{g}^{-1}$ , respectively. The specific surface area of the as-prepared composite has been significantly improved, which could be in favor of enhancing the gas-sensing properties.

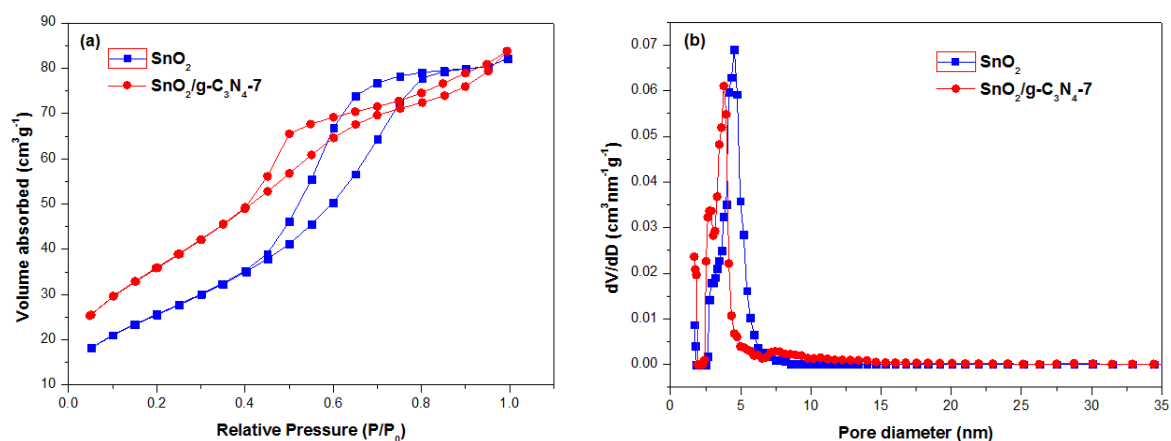
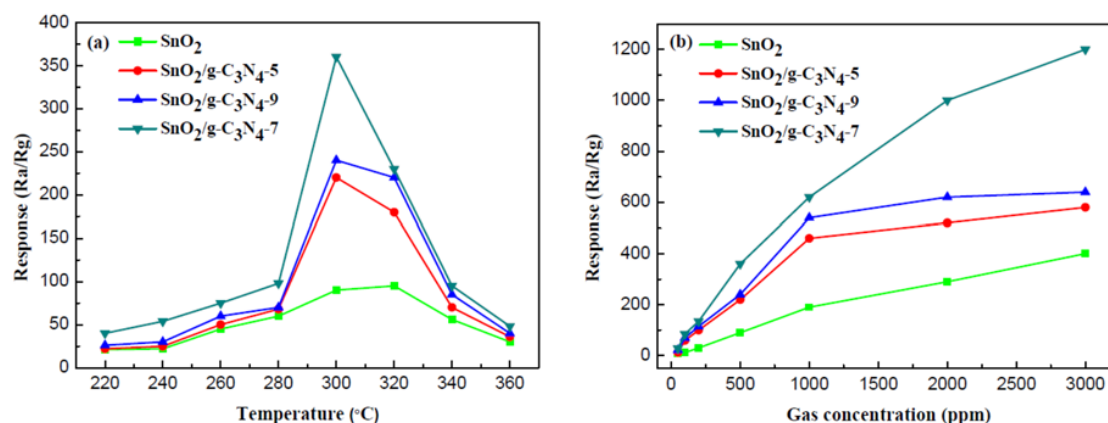


**Figure 5.** (a)  $N_2$  adsorption-desorption isotherms and (b) the corresponding pore size distribution curves of the  $SnO_2$  and  $SnO_2/g-C_3N_4$ -7 composite.

## 2.2. Gas-Sensing Performance

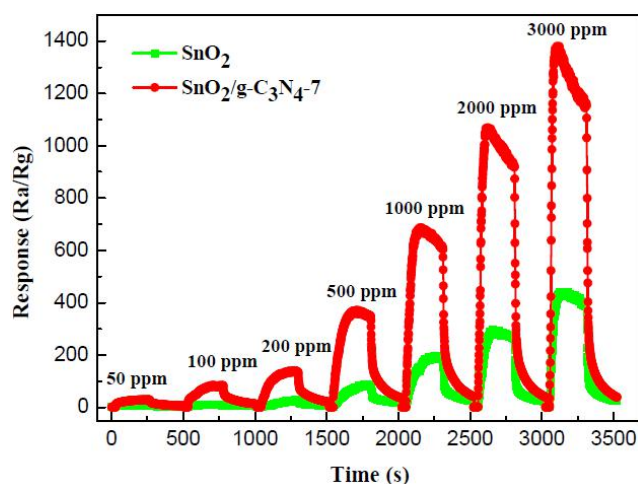
The gas-sensing properties of the as-prepared samples in relation ethanol were investigated, in detail. Figure 6a shows the response values of pure  $SnO_2$  and  $SnO_2/g-C_3N_4$ -based sensors to 500 ppm ethanol at different operating temperatures. It can be clearly observed from the line chart of the three  $SnO_2/g-C_3N_4$  samples that the response values increase with the increase of the operating temperature under  $300^\circ\text{C}$ . However, the response values decrease when the temperature is above  $300^\circ\text{C}$ . The maximum response of  $SnO_2/g-C_3N_4$ -7 is 360 at  $300^\circ\text{C}$ . In stark contrast, the maximum response of the pure  $SnO_2$  is only 95 at  $320^\circ\text{C}$ . This phenomenon can be explained by the fact that the  $SnO_2/g-C_3N_4$ -7-based sensor can tend to the balance between the speeds of chemical adsorption and desorption at a lower temperature, and reach a higher response than that of the pure  $SnO_2$  sensor. This result indicates that the  $SnO_2/g-C_3N_4$ -based sensor has a great influence and enhances the gas-sensing properties for ethanol. It reaches the maximum response when the mass percentage of  $g-C_3N_4$  in the composites is 7%. The specific surface area of the  $SnO_2$ ,  $SnO_2/g-C_3N_4$ -5,  $SnO_2/g-C_3N_4$ -7, and  $SnO_2/g-C_3N_4$ -9 composites is  $94.3 \text{ m}^2 \cdot \text{g}^{-1}$ ,  $113.8 \text{ m}^2 \cdot \text{g}^{-1}$ ,  $132.5 \text{ m}^2 \cdot \text{g}^{-1}$ , and  $122.2 \text{ m}^2 \cdot \text{g}^{-1}$ , respectively. When the  $g-C_3N_4$  content in the composites exceeds a certain value (e.g., 7 wt % in this work), it may form the connection of bulk. As a result, the specific surface area of the composite will decrease and there will be a reduced number of active sites for the adsorption of oxygen and ethanol gas, leading to the degradation of gas-sensing properties. Consequently, the gas sensor performance increases at first and decreases when the  $g-C_3N_4$  content in the composites increases. A suitable amount of  $g-C_3N_4$  in the composite is beneficial to the dispersity, and a preferable heterojunctional structure can be formed in the interface region between 2D  $g-C_3N_4$  and  $SnO_2$ . A high content of 2D  $g-C_3N_4$  may lead to the connection of the  $g-C_3N_4$  nanosheets, which could form micro electric bridges

on the surface. The micro electric bridges may result in the semiconductor's resistance being reduced, causing a reduction in the gas sensor performance. Figure 6b displays the response values of the four samples at 300 °C to different concentrations of ethanol. As shown in the line chart, the response values increase with the increasing ethanol concentrations. The slope of the curves increases rapidly when the concentration range of ethanol is from 50 ppm to 500 ppm. However, it increases slowly gradually with an increasing concentration in the range of 500–3000 ppm. Furthermore, the responses of the SnO<sub>2</sub>/g-C<sub>3</sub>N<sub>4</sub> sensors are much higher than that of pure SnO<sub>2</sub>. It can be concluded that the adsorption of ethanol has approached the saturation value when the concentration reaches 3000 ppm.



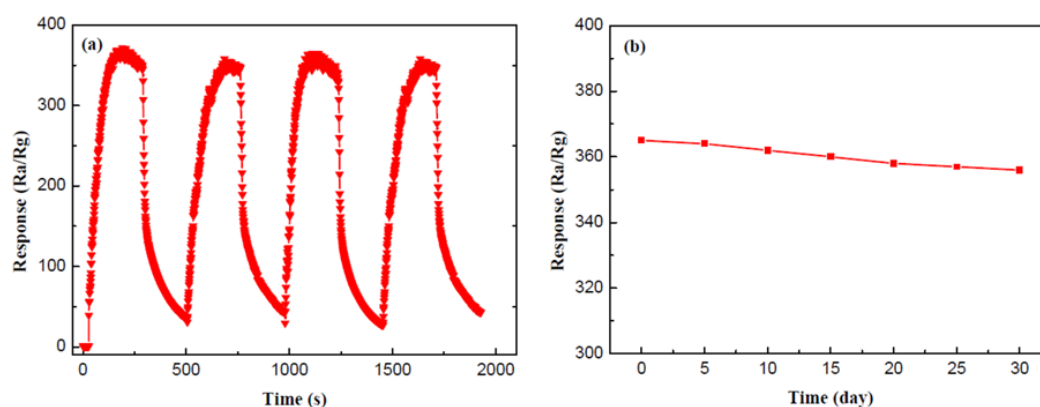
**Figure 6.** (a) Response values of the sensors based on SnO<sub>2</sub>, SnO<sub>2</sub>/g-C<sub>3</sub>N<sub>4</sub>-5, SnO<sub>2</sub>/g-C<sub>3</sub>N<sub>4</sub>-7, and SnO<sub>2</sub>/g-C<sub>3</sub>N<sub>4</sub>-9 to 500 ppm ethanol as a function of the operating temperature; (b) the responses of sensors (SnO<sub>2</sub>, SnO<sub>2</sub>/g-C<sub>3</sub>N<sub>4</sub>-5, SnO<sub>2</sub>/g-C<sub>3</sub>N<sub>4</sub>-7, and SnO<sub>2</sub>/g-C<sub>3</sub>N<sub>4</sub>-9) operated at 300 °C versus different concentrations of ethanol.

Figure 7 displays the real time successive response-recover curves of the pure SnO<sub>2</sub> and SnO<sub>2</sub>/g-C<sub>3</sub>N<sub>4</sub>-7 to 500 ppm ethanol in the range of 50–3000 ppm at 300 °C. As shown by the curves, the response values of both sensors increase with the increasing concentration. The response value of the SnO<sub>2</sub>/g-C<sub>3</sub>N<sub>4</sub>-7-based sensor is much higher than that of the pure SnO<sub>2</sub>-based sensor to the same concentration of ethanol. The gas-sensing properties of the composites enhanced a lot, which is consistent with the expected.



**Figure 7.** Real time response curves of the pure SnO<sub>2</sub> and SnO<sub>2</sub>/g-C<sub>3</sub>N<sub>4</sub>-7 to ethanol in the range of 50–3000 ppm.

The repeatability and stability are both crucial criteria to measure the gas-sensing properties. Figure 8a reveals the repeatability of the  $\text{SnO}_2/\text{g-C}_3\text{N}_4$ -7 sensor to 500 ppm ethanol at 300 °C. As shown by the curves, the response values of the four response-recovery cycles are almost maintained at about 360. It can be concluded that the composite sensor has an admirable repeatability for ethanol gas sensing. A durable response value was measured to explore the stability of the  $\text{SnO}_2/\text{g-C}_3\text{N}_4$ -7 sensor. Figure 8b displays the test result every five days, and the response values to 500 ppm ethanol at 300 °C are maintained at around 360. Therefore, we may safely draw the conclusion that the  $\text{SnO}_2/\text{g-C}_3\text{N}_4$ -7-based sensor has an unexceptionable stability for ethanol gas sensing.



**Figure 8.** (a) Repeatability and (b) stability measurements of the  $\text{SnO}_2/\text{g-C}_3\text{N}_4$ -7-based sensor to 500 ppm ethanol at 300 °C.

It is generally known that selectivity is another key criterion of gas sensors. Figure 9 summarizes the selectivity test results of the pure  $\text{SnO}_2$  and  $\text{SnO}_2/\text{g-C}_3\text{N}_4$ -7 sensors to five different gases of 500 ppm, including methanol, ethanol, toluene, formaldehyde, and acetone. It can be seen that the  $\text{SnO}_2/\text{g-C}_3\text{N}_4$ -7 sensor exhibits a higher response to ethanol than to other gases compared to the pure  $\text{SnO}_2$  sensor. The higher responses to ethanol may be because ethanol is more likely to lose electrons in the process of the redox reaction with the absorbed oxygen and hydroxyl group ( $-\text{OH}$ ) and is much easier to oxidize at the optimum operating temperature [35].

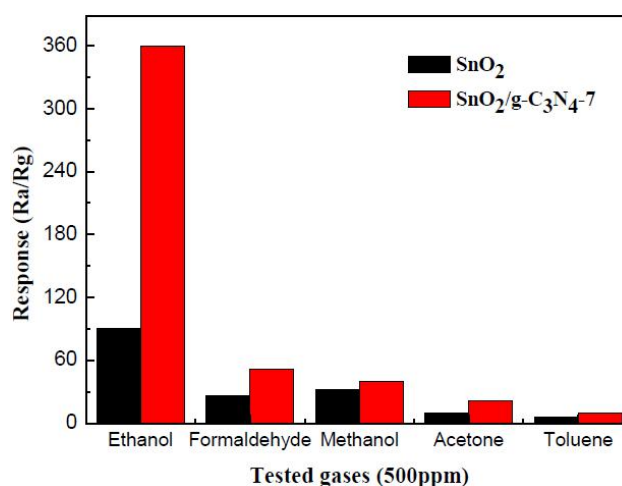


**Figure 9.** Responses of  $\text{SnO}_2$  and  $\text{SnO}_2/\text{g-C}_3\text{N}_4$ -7-based sensors to 500 ppm different reducing gases at 300 °C.

The gas-sensing performance of different sensing materials when using ethanol is listed in Table 1. As can be seen from Table 1, the response values of  $\text{Fe}_2\text{O}_3$  nanoparticles coated with  $\text{SnO}_2$

nanowires [14],  $\alpha$ -Fe<sub>2</sub>O<sub>3</sub>/g-C<sub>3</sub>N<sub>4</sub> [35], RGO-SnO<sub>2</sub> [36], and Au/SnO<sub>2</sub> [37] were 31.18, 7.76, 70.4, and 18, respectively. In this work, the response value of SnO<sub>2</sub>/g-C<sub>3</sub>N<sub>4</sub>-7 to 100 ppm of ethanol vapor was 85 at 300 °C. Therefore, the SnO<sub>2</sub>/g-C<sub>3</sub>N<sub>4</sub> composites show an excellent sensing property to ethanol vapor, and thus have a great potential application.

**Table 1.** Gas-sensing performance comparison of various gas sensors toward ethanol.

Sensing Materials	Ethanol Concentration (ppm)	Temperature (°C)	Response (R <sub>a</sub> /R <sub>g</sub> )	Ref.
Fe <sub>2</sub> O <sub>3</sub> -SnO <sub>2</sub>	100	300	31.18	[14]
$\alpha$ -Fe <sub>2</sub> O <sub>3</sub> /g-C <sub>3</sub> N <sub>4</sub>	100	340	7.76	[35]
RGO-SnO <sub>2</sub>	100	300	70.4	[36]
Au/SnO <sub>2</sub>	100	340	18	[37]
SnO <sub>2</sub> /g-C <sub>3</sub> N <sub>4</sub>	100	300	85	this work

As displayed in Figure 10a, the absorption edge of SnO<sub>2</sub>, SnO<sub>2</sub>/g-C<sub>3</sub>N<sub>4</sub>-7 and g-C<sub>3</sub>N<sub>4</sub> are around 377 nm, 441 nm, and 455 nm, respectively. This result can be ascribed to the heterojunction structure between SnO<sub>2</sub> and g-C<sub>3</sub>N<sub>4</sub>. The band gap energies of SnO<sub>2</sub> and g-C<sub>3</sub>N<sub>4</sub> can be estimated according to the equation ( $Ah\nu = k(h\nu - E_g)^{n/2}$ ). In this equation,  $n$  is determined by the type of optical transition of a semiconductor. The value for g-C<sub>3</sub>N<sub>4</sub> and SnO<sub>2</sub> is 4 and 1, respectively.  $A$ ,  $\nu$ ,  $E_g$ ,  $k$  and  $h$  are the absorption coefficient, light frequency, Planck constant, band gap and a constant, respectively. The diagrams are shown in Figure 10b,c. The  $E_g$  of SnO<sub>2</sub>/g-C<sub>3</sub>N<sub>4</sub>-7 should be roughly calculated according to the equation ( $E_g = 1240/\lambda$ ) because of the uncertain type of optical transition. As a result, the  $E_g$  of SnO<sub>2</sub>, g-C<sub>3</sub>N<sub>4</sub>, and SnO<sub>2</sub>/g-C<sub>3</sub>N<sub>4</sub>-7 are 3.49 eV, 2.75 eV, and 2.81 eV, respectively.

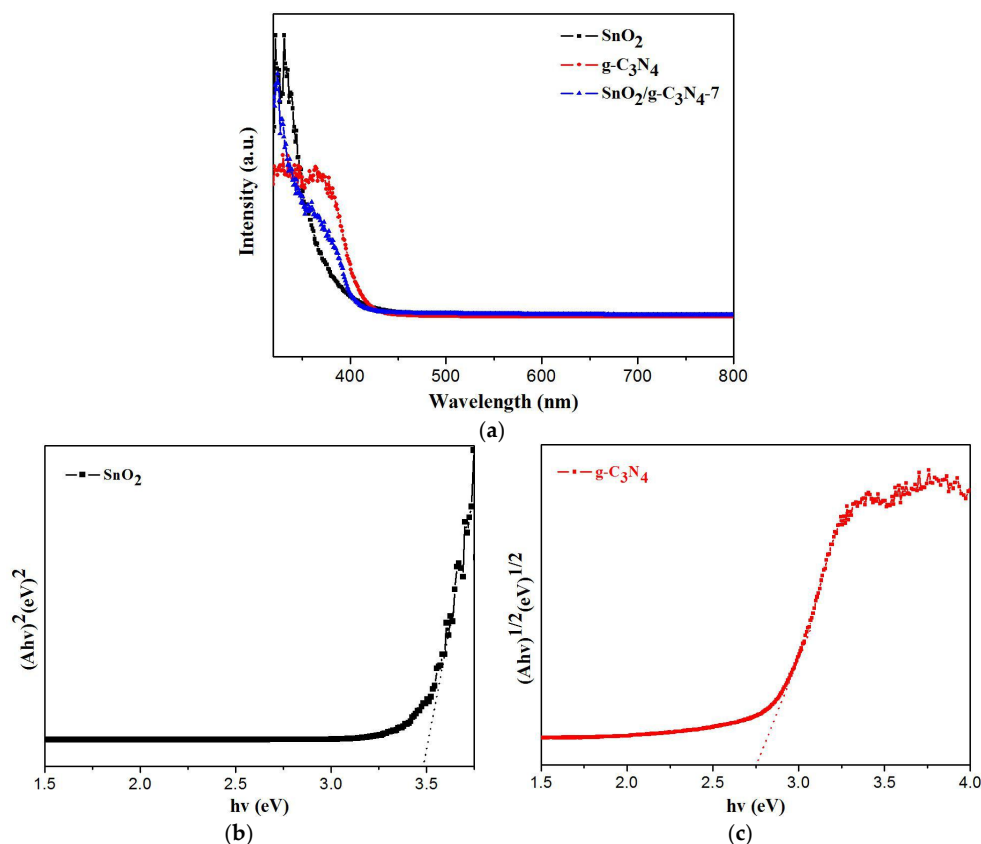
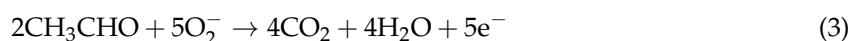
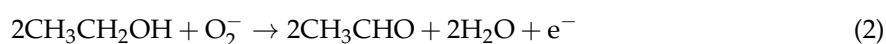


**Figure 10.** (a) UV-vis diffuse reflectance spectra of SnO<sub>2</sub>, g-C<sub>3</sub>N<sub>4</sub>, and SnO<sub>2</sub>/g-C<sub>3</sub>N<sub>4</sub>-7 composites, (b) plot of  $(Ah\nu)^2$  versus energy ( $h\nu$ ) for the band gap energy of SnO<sub>2</sub>, (c) plot of  $(Ah\nu)^{1/2}$  versus energy ( $h\nu$ ) for the band gap energy of g-C<sub>3</sub>N<sub>4</sub>.

The sensing mechanism of the SnO<sub>2</sub>/g-C<sub>3</sub>N<sub>4</sub> composite towards ethanol gas need to be further investigated. When the sensor was exposed in air, oxygen molecules were adsorbed on the surface of SnO<sub>2</sub> and capture electrons from the conduction band of SnO<sub>2</sub>. Then oxygen molecules were ionized to O<sup>2-</sup>, O<sup>-</sup>, and O<sub>2</sub><sup>-</sup>, and the formation of depletion layers led to the increase in the resistance of the composite sensor. However, when the sensor was exposed to the ethanol gas, the ethanol molecules proceeded oxidation and the reduction reaction with oxygen ions absorbed on the surface of the sensor. Concurrently, the ethanol molecules were oxidized into acetaldehyde and eventually turned into carbon dioxide and water [24]. As a result, the trapped electrons were released back to the depletion layer of the sensing film, resulting in the decrease in the resistance of the composite-based sensor. The SnO<sub>2</sub>/g-C<sub>3</sub>N<sub>4</sub> composite exhibited more preferable gas-sensing properties than that of pure SnO<sub>2</sub>. This is mainly due to the high specific surface area and the interaction between g-C<sub>3</sub>N<sub>4</sub> and SnO<sub>2</sub>. The presence of g-C<sub>3</sub>N<sub>4</sub> can prevent the aggregation of SnO<sub>2</sub> particles to form a high surface approachability structure, leading to the promotion of the adsorption and diffusion process of ethanol molecules. In this composite, the s-triazine structure g-C<sub>3</sub>N<sub>4</sub> sheet substrate can provide more active sites to adsorb O<sub>2</sub> molecules. The elevated gas-sensing properties may also be due to the interactions between Sn and g-C<sub>3</sub>N<sub>4</sub>, and the heterojunction of the interface region between g-C<sub>3</sub>N<sub>4</sub> and SnO<sub>2</sub>. The electrical property at the heterojunction changes when ethanol gas molecules pass through the interface region between g-C<sub>3</sub>N<sub>4</sub> and SnO<sub>2</sub>. Both SnO<sub>2</sub> and g-C<sub>3</sub>N<sub>4</sub> are n-type semiconductors. The band gaps are 3.71 eV and 2.7 eV, respectively. The conduction band level of g-C<sub>3</sub>N<sub>4</sub> is more negative than SnO<sub>2</sub>. When SnO<sub>2</sub> and g-C<sub>3</sub>N<sub>4</sub> were combined, they formed a heterojunction structure. The electrons will thus inflow from the conduction band of g-C<sub>3</sub>N<sub>4</sub> to the conduction band of SnO<sub>2</sub>, leading to a higher potential barrier. As a result, the electrons and holes are separated [38]. Meanwhile, the heterojunction structure may suppress the recombination of the electron-hole and urge electrons to quickly transfer from the ethanol vapor to the surface of SnO<sub>2</sub>/g-C<sub>3</sub>N<sub>4</sub>. Therefore, this leads to a higher response because of the increased conductivity of the heterojunction structure [35]. This co-adjacent retiform structure could provide more accesses for the gas adsorption and diffusion between SnO<sub>2</sub> and ethanol molecules.



### 3. Materials and Methods

#### 3.1. Chemicals

Urea and Tin (IV) chloride pentahydrate (SnCl<sub>4</sub>·5H<sub>2</sub>O, 99.0%) were purchased from Macklin Biochemical Co., Ltd. (Shanghai, China). All chemicals were used as received, without further purification.

#### 3.2. Preparation of g-C<sub>3</sub>N<sub>4</sub>

Graphitic carbon nitride (g-C<sub>3</sub>N<sub>4</sub>) was directly synthesized by the pyrolysis of urea in the muffle furnace (Luoyang Shenjia Kiln Co., Ltd., Luoyang, Henan, China). A total of 20 g urea was put into an alumina crucible with a cover and then warmed to a temperature of 250 °C within 110 min, before being kept at 250 °C for 1 h. Then, the temperature was increased to 350 °C within 50 min and kept at 350 °C for 2 h. Finally, temperature rose to 550 °C within 100 min and was kept at 550 °C for another 2 h. The heating rate of the whole reaction was 2 °C·min<sup>-1</sup>. The resulting yellow powder was collected.

#### 3.3. Synthesis of the SnO<sub>2</sub>/g-C<sub>3</sub>N<sub>4</sub> Composite

SnO<sub>2</sub>/g-C<sub>3</sub>N<sub>4</sub> composites were synthesized through a facile calcination method. In a typical preparation process, a certain amount g-C<sub>3</sub>N<sub>4</sub> was dissolved in 100 mL H<sub>2</sub>O and 2.09 g SnCl<sub>4</sub>·5H<sub>2</sub>O

was added into the dispersed suspension with ultrasonic treatment for 2 h. Then, the mixed solution was transferred into an alumina crucible and put it into the muffle furnace. It was heated to 400 °C for 2 h. Finally, the resulting product was ground to powder. According to this method, the different mass ratios of the SnO<sub>2</sub>/g-C<sub>3</sub>N<sub>4</sub> composites were synthesized and marked as SnO<sub>2</sub>/g-C<sub>3</sub>N<sub>4</sub>-5, SnO<sub>2</sub>/g-C<sub>3</sub>N<sub>4</sub>-7, and SnO<sub>2</sub>/g-C<sub>3</sub>N<sub>4</sub>-9. For comparison, the same method was used to synthesize the pure SnO<sub>2</sub> particles with the absence of g-C<sub>3</sub>N<sub>4</sub>.

### 3.4. Characterizations

The samples were characterized by X-ray diffraction (XRD, Bruker-AXS D8, Bruker, Madison, WI, USA) with Cu K $\alpha$  radiation at 40 kV and 25 mA. The structure and morphology of the samples were observed by field-emission scanning electron microscopy (FESEM, Quanta™ 250 FEG) (FEI, Eindhoven, The Netherlands). Transmission electron microscopy (TEM) analysis was performed on a JEOL JEM-2100 microscope (JEOL, Tokyo, Japan) operating at 200 kV. The thermal gravity and differential thermal analysis (TG-DTA) was carried on TA-SDT Q600 (TA, New Castle, DE, USA) at a heating rate 10 °C·min<sup>-1</sup> under an air atmosphere. Nitrogen adsorption-desorption isotherms were obtained on a Quantachrome Autosorb-iQ sorption analyzer (Quantachrome, Boynton Beach, FL, USA). Before carrying out the measurement, the samples were degassed for more than 6 h at 300 °C.

### 3.5. Gas-Sensing Test

The gas-sensing performance of the as-synthesized samples when using ethanol was tested by using the intelligent gas-sensing analysis system of CGS-4TPS (Beijing Elite Co., Ltd., Beijing, China). Figure 11 shows a brief schematic diagram of the device. The gas sensors were prepared according to the usual way. A small amount of the as-prepared sample was fully ground in agate mortar with a few drops ethanol, which served as the agglomerant to form starchiness. Afterwards, the pastes were equably spread on the ceramic substrate (13.4 mm × 7 mm) with interdigitated Ag-Pd electrodes to form the thin film. Before carrying out the test, the substrate was aged at 180 °C for 24 h to improve the stability and repeatability of the gas sensors. The response of the sensors was defined as the ratio of  $R_a/R_g$ , where  $R_a$  and  $R_g$  were the resistance of sensor in air and in the target gas, respectively.

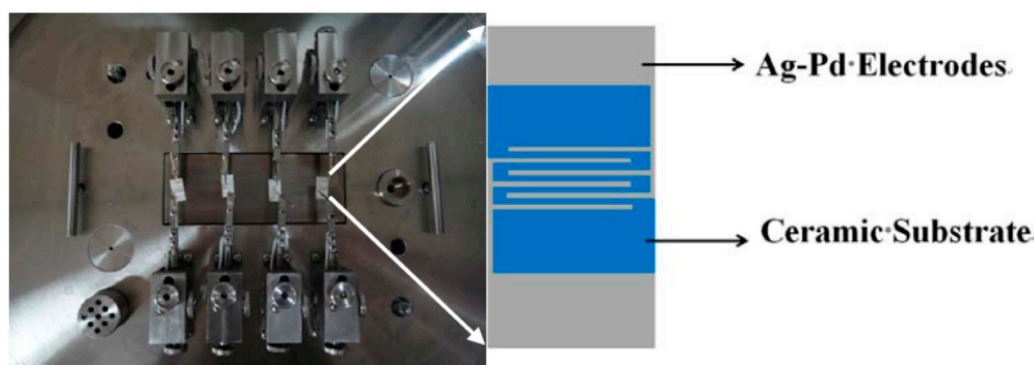


**Figure 11.** The internal structure diagram of the CGS-4TPS gas-sensing test system and the structure of the substrate.

## 4. Conclusions

In this study, the SnO<sub>2</sub>/g-C<sub>3</sub>N<sub>4</sub> composites with a high surface area (132.5 m<sup>2</sup>·g<sup>-1</sup>) were synthesized via a facile calcination method by using SnCl<sub>4</sub>·5H<sub>2</sub>O and urea as the precursor. The SnO<sub>2</sub> particles were highly distributed on the g-C<sub>3</sub>N<sub>4</sub> nanosheets. The gas-sensing properties of the SnO<sub>2</sub>/g-C<sub>3</sub>N<sub>4</sub>-7 composite-based sensor exhibited preferable results when compared to the pure SnO<sub>2</sub>, including the sensitivity and selectivity. Considering the easy-preparation process, the SnO<sub>2</sub>/g-C<sub>3</sub>N<sub>4</sub> composite could be a promising candidate for high-performance ethanol gas-sensing applications.

**Acknowledgments:** This work was supported by the National Natural Science Foundation of China (51404097, 51504083, U1404613), Program for Science & Technology Innovation Talents in Universities of Henan Province (17HASTIT029), Natural Science Foundation of Henan Province of China (162300410113), Project funded by China Postdoctoral Science Foundation (2016M592290), the Research Foundation for Youth Scholars of Higher Education of Henan Province (2016GGJS-040), the Fundamental Research Funds for the Universities of Henan Province (NSFRF1606, NSFRF1614); Program for Innovative Research Team (in Science and Technology) in the University of Henan Province (16IRTSTHN005), and Foundation for Distinguished Young Scientists of Henan Polytechnic University (J2016-2, J2017-3).

**Author Contributions:** Jianliang Cao conceived and designed the experiments; Cong Qin, Bo Zhang, Yuxiao Gong, Huoli Zhang, Guang Sun, and Hari Bala performed the experiments and analyzed the data; Yan Wang and Zhanying Zhang provided the concept of this research and managed all the experimental and writing process as the corresponding authors; all authors discussed the results and commented on the manuscript.

**Conflicts of Interest:** The authors declare no conflict of interest.

## References

1. Hou, C.; Li, J.; Huo, D.; Luo, X.; Dong, J.; Yang, M.; Shi, X. A portable embedded toxic gas detection device based on a cross-responsive sensor array. *Sens. Actuators B* **2012**, *161*, 244–250. [[CrossRef](#)]
2. Schedin, F.; Geim, A.K.; Morozov, S.V.; Hill, E.W.; Blake, P.; Katsnelson, M.I.; Novoselov, K.S. Detection of individual gas molecules adsorbed on graphene. *Nat. Mater.* **2007**, *6*, 652–655. [[CrossRef](#)] [[PubMed](#)]
3. Ariyageadsakul, P.; Vchirawongkwin, V.; Kritayakornpong, C. Determination of toxic carbonyl species including acetone, formaldehyde, and phosgene by polyaniline emeraldine gas sensor using DFT calculation. *Sens. Actuators B* **2016**, *232*, 165–174. [[CrossRef](#)]
4. Hui, G.H. Detection of Sulfur Hexafluoride Based on Stochastic Resonance and Miniaturized Sensor Array. *Chin. J. Anal. Chem.* **2010**, *38*, 984–988.
5. Kaneti, Y.V.; Yue, J.; Moriceau, J.; Chen, C.; Liu, M.; Yuan, Y.; Jiang, X.; Yu, A. Experimental and theoretical studies on noble metal decorated tin oxide flower-like nanorods with high ethanol sensing performance. *Sens. Actuators B* **2015**, *219*, 83–93. [[CrossRef](#)]
6. Kumar, N.; Srivastava, A.K.; Patel, H.S.; Gupta, B.K.; Varma, G.D. Facile Synthesis of ZnO–Reduced Graphene Oxide Nanocomposites for NO<sub>2</sub> Gas Sensing Applications. *Eur. J. Inorg. Chem.* **2015**, *2015*, 1912–1923. [[CrossRef](#)]
7. Bhuvaneshwari, S.; Gopalakrishnan, N. Hydrothermally synthesized Copper Oxide (CuO) superstructures for ammonia sensing. *J. Colloid Interface Sci.* **2016**, *480*, 76–84. [[CrossRef](#)] [[PubMed](#)]
8. Mirzaei, A.; Janghorban, K.; Hashemi, B.; Bonavita, A.; Bonyani, M.; Leonardi, S.G.; Neri, G. Synthesis, Characterization and Gas Sensing Properties of Ag@alpha-Fe<sub>2</sub>O<sub>3</sub> Core-Shell Nanocomposites. *Nanomaterials* **2015**, *5*, 737–749. [[CrossRef](#)] [[PubMed](#)]
9. Deng, S.; Liu, X.; Chen, N.; Deng, D.; Xiao, X.; Wang, Y. A highly sensitive VOC gas sensor using p-type mesoporous Co<sub>3</sub>O<sub>4</sub> nanosheets prepared by a facile chemical coprecipitation method. *Sens. Actuators B* **2016**, *233*, 615–623. [[CrossRef](#)]
10. Yang, C.; Deng, W.; Liu, H.; Ge, S.; Yan, M. Turn-on fluorescence sensor for glutathione in aqueous solutions using carbon dots-MnO<sub>2</sub> nanocomposites. *Sens. Actuators B* **2015**, *216*, 286–292. [[CrossRef](#)]
11. An, X.; Yu, J.C.; Wang, Y.; Hu, Y.; Yu, X.; Zhang, G. WO<sub>3</sub> nanorods/graphene nanocomposites for high-efficiency visible-light-driven photocatalysis and NO<sub>2</sub> gas sensing. *J. Mater. Chem.* **2012**, *22*, 8525–8531. [[CrossRef](#)]
12. Xue, P.; Yang, X.; Lai, X.; Xia, W.; Li, P.; Fang, J. Controlling synthesis and gas-sensing properties of ordered mesoporous In<sub>2</sub>O<sub>3</sub>-reduced graphene oxide (rGO) nanocomposite. *Sci. Bull.* **2015**, *60*, 1348–1354. [[CrossRef](#)]
13. Lin, L.; Liu, T.; Yu, W.; Guo, Z.; Zeng, W. Synthesis of multifarious hierarchical flower-like NiO and their gas-sensing properties. *Mater. Res. Bull.* **2013**, *48*, 2730–2736. [[CrossRef](#)]
14. Choi, K.S.; Park, S.; Chang, S.-P. Enhanced ethanol sensing properties based on SnO<sub>2</sub> nanowires coated with Fe<sub>2</sub>O<sub>3</sub> nanoparticles. *Sens. Actuators B* **2017**, *238*, 871–879. [[CrossRef](#)]
15. Li, Y.; Chen, N.; Deng, D.; Xing, X.; Xiao, X.; Wang, Y. Formaldehyde detection: SnO<sub>2</sub> microspheres for formaldehyde gas sensor with high sensitivity, fast response/recovery and good selectivity. *Sens. Actuators B* **2017**, *238*, 264–273. [[CrossRef](#)]

16. Zhang, D.; Liu, A.; Chang, H.; Xia, B. Room-temperature high-performance acetone gas sensor based on hydrothermal synthesized SnO<sub>2</sub>-reduced graphene oxide hybrid composite. *RSC Adv.* **2015**, *5*, 3016–3022. [[CrossRef](#)]
17. Srivastava, V.; Jain, K. At room temperature graphene/SnO<sub>2</sub> is better than MWCNT/SnO<sub>2</sub> as NO<sub>2</sub> gas sensor. *Mater. Lett.* **2016**, *169*, 28–32. [[CrossRef](#)]
18. Guo, D.; Cai, P.; Sun, J.; He, W.; Wu, X.; Zhang, T.; Wang, X.; Zhang, X. Reduced-graphene-oxide/metal-oxide p-n heterojunction aerogels as efficient 3D sensing frameworks for phenol detection. *Carbon* **2016**, *99*, 571–578. [[CrossRef](#)]
19. Latif, U.; Dickert, F.L. Graphene Hybrid Materials in Gas Sensing Applications. *Sensors* **2015**, *15*, 30504–30524. [[CrossRef](#)] [[PubMed](#)]
20. Yi, Y.; Zhu, G.; Sun, H.; Sun, J.; Wu, X. Nitrogen-doped hollow carbon spheres wrapped with graphene nanostructure for highly sensitive electrochemical sensing of parachlorophenol. *Biosens. Bioelectron.* **2016**, *86*, 62–67. [[CrossRef](#)] [[PubMed](#)]
21. Song, Z.; Wei, Z.; Wang, B.; Luo, Z.; Xu, S.; Zhang, W.; Yu, H.; Li, M.; Huang, Z.; Zang, J.; et al. Sensitive Room-Temperature H<sub>2</sub>S Gas Sensors Employing SnO<sub>2</sub> Quantum Wire/Reduced Graphene Oxide Nanocomposites. *Chem. Mater.* **2016**, *28*, 1205–1212. [[CrossRef](#)]
22. Mao, S.; Cui, S.; Lu, G.; Yu, K.; Wen, Z.; Chen, J. Tuning gas-sensing properties of reduced graphene oxide using tin oxide nanocrystals. *J. Mater. Chem.* **2012**, *22*, 11009–11013. [[CrossRef](#)]
23. Zhang, H.; Feng, J.; Fei, T.; Liu, S.; Zhang, T. SnO<sub>2</sub> nanoparticles-reduced graphene oxide nanocomposites for NO<sub>2</sub> sensing at low operating temperature. *Sens. Actuators B* **2014**, *190*, 472–478. [[CrossRef](#)]
24. Zhang, D.; Liu, J.; Chang, H.; Liu, A.; Xia, B. Characterization of a hybrid composite of SnO<sub>2</sub> nanocrystal-decorated reduced graphene oxide for ppm-level ethanol gas sensing application. *RSC Adv.* **2015**, *5*, 18666–18672. [[CrossRef](#)]
25. Mamba, G.; Mishra, A.K. Graphitic carbon nitride (g-C<sub>3</sub>N<sub>4</sub>) nanocomposites: A new and exciting generation of visible light driven photocatalysts for environmental pollution remediation. *Appl. Catal. B* **2016**, *198*, 347–377. [[CrossRef](#)]
26. Shao, L.; Jiang, D.; Xiao, P.; Zhu, L.; Meng, S.; Chen, M. Enhancement of g-C<sub>3</sub>N<sub>4</sub> nanosheets photocatalysis by synergistic interaction of ZnS microsphere and RGO inducing multistep charge transfer. *Appl. Catal. B* **2016**, *198*, 200–210. [[CrossRef](#)]
27. Hu, Y.; Li, L.; Zhang, L.; Lv, Y. Dielectric barrier discharge plasma-assisted fabrication of g-C<sub>3</sub>N<sub>4</sub>-Mn<sub>3</sub>O<sub>4</sub> composite for high-performance cataluminescence H<sub>2</sub>S gas sensor. *Sens. Actuators B* **2017**, *239*, 1177–1184. [[CrossRef](#)]
28. Dai, H.; Zhang, S.; Xu, G.; Peng, Y.; Gong, L.; Li, X.; Li, Y.; Lin, Y.; Chen, G. Highly photoactive heterojunction based on g-C<sub>3</sub>N<sub>4</sub> nanosheets decorated with dendritic zinc(II) phthalocyanine through axial coordination and its ultrasensitive enzyme-free sensing of choline. *RSC Adv.* **2014**, *4*, 58226–58230. [[CrossRef](#)]
29. Chen, P.W.; Li, K.; Yu, Y.X.; Zhang, W.D. Cobalt-doped graphitic carbon nitride photocatalysts with high activity for hydrogen evolution. *Appl. Surf. Sci.* **2017**, *392*, 608–615. [[CrossRef](#)]
30. Wei, J.; Huang, C.; Wu, H.; Kan, E. High-capacity hydrogen storage in Li-adsorbed g-C<sub>3</sub>N<sub>4</sub>. *Mater. Chem. Phys.* **2016**, *180*, 440–444. [[CrossRef](#)]
31. Carvalho, K.T.G.; Nogueira, A.E.; Lopes, O.F.; Byzynski, G.; Ribeiro, C. Synthesis of g-C<sub>3</sub>N<sub>4</sub>/Nb<sub>2</sub>O<sub>5</sub> heterostructures and their application in the removal of organic pollutants under visible and ultraviolet irradiation. *Ceram. Int.* **2017**, *43*, 3521–3530. [[CrossRef](#)]
32. Zeng, B.; Zhang, L.; Wan, X.; Song, H.; Lv, Y. Fabrication of α-Fe<sub>2</sub>O<sub>3</sub>/g-C<sub>3</sub>N<sub>4</sub> composites for cataluminescence sensing of H<sub>2</sub>S. *Sens. Actuators B* **2015**, *211*, 370–376. [[CrossRef](#)]
33. Zhang, X.L.; Zheng, C.; Guo, S.S.; Li, J.; Yang, H.H.; Chen, G. Turn-on fluorescence sensor for intracellular imaging of glutathione using g-C<sub>3</sub>N<sub>4</sub> nanosheet-MnO<sub>2</sub> sandwich nanocomposite. *Anal. Chem.* **2014**, *86*, 3426–3434. [[CrossRef](#)] [[PubMed](#)]
34. She, X.; Xu, H.; Wang, H.; Xia, J.; Song, Y.; Yan, J.; Xu, Y.; Zhang, Q.; Du, D.; Li, H. Controllable synthesis of CeO<sub>2</sub>/g-C<sub>3</sub>N<sub>4</sub> composites and their applications in the environment. *Dalton Trans.* **2015**, *44*, 7021–7031. [[CrossRef](#)] [[PubMed](#)]
35. Zhang, Y.; Zhang, D.; Guo, W.; Chen, S. The α-Fe<sub>2</sub>O<sub>3</sub>/g-C<sub>3</sub>N<sub>4</sub> heterostructural nanocomposites with enhanced ethanol gas sensing performance. *J. Alloy. Compd.* **2016**, *685*, 84–90. [[CrossRef](#)]

36. Zito, C.A.; Perfecto, T.M.; Volanti, D.P. Impact of reduced graphene oxide on the ethanol sensing performance of hollow SnO<sub>2</sub> nanoparticles under humid atmosphere. *Sens. Actuators B* **2017**, *244*, 466–474. [[CrossRef](#)]
37. Guo, J.; Zhang, J.; Gong, H.; Ju, D.; Cao, B. Au nanoparticle-functionalized 3D SnO<sub>2</sub> microstructures for high performance gas sensor. *Sens. Actuators B* **2016**, *226*, 266–272. [[CrossRef](#)]
38. Zang, Y.; Li, L.; Li, X.; Lin, R.; Li, G. Synergistic collaboration of g-C<sub>3</sub>N<sub>4</sub>/SnO<sub>2</sub> composites for enhanced visible-light photocatalytic activity. *Chem. Eng. J.* **2014**, *246*, 277–286. [[CrossRef](#)]



© 2017 by the authors. Licensee MDPI, Basel, Switzerland. This article is an open access article distributed under the terms and conditions of the Creative Commons Attribution (CC BY) license (<http://creativecommons.org/licenses/by/4.0/>).